Predicting Effective Conductivities Based on Geometric Microstructure Characteristics

Ole Stenzel, Omar Pecho and Lorenz Holzer

Institute of Computational Physics, ZHAW Winterthur, 8400 Winterthur, Switzerland

Matthias Neumann and Volker Schmidt

Institute of Stochastics, Ulm University, 89069 Ulm, Germany

Abstract

Empirical relationships between effective conductivities in porous and composite materials and their geometric characteristics such as volume fraction ε, tortuosity τ and constrictivity β are established. For this purpose, 43 virtually generated 3D microstructures with varying geometric characteristics are considered. Effective conductivities σ_{eff} are determined by numerical transport simulations. Using error-minimization the following relationships have been established: $\sigma_{\text{eff}} = \sigma_0 \frac{\varepsilon^{1.15}\beta^{0.37}}{\tau_{\text{geod}}^{4.39}}$ and $\sigma_{\text{eff}} = \sigma_0 \frac{\varepsilon\beta^{0.36}}{\tau_{\text{geod}}^{5.17}}$ (simplified formula) with intrinsic conductivity σ_0, geodesic tortuosity τ_{geod} and relative prediction errors of 19% and 18%, respectively. We critically analyze the methodologies used to determine tortuosity and constrictivity. Comparing geometric tortuosity and geodesic tortuosity, our results indicate that geometric tortuosity has a tendency to overestimate the windedness of transport paths. Analyzing various definitions of constrictivity, we find that the established definition describes the effect of bottlenecks well. In summary, the established relationships are important for a purposeful optimization of materials with specific transport properties, such as porous electrodes in fuel cells and batteries.

Keywords: *effective conductivity, predictive analytics, porous media, constrictivity, geometric tortuosity, geodesic tortuosity, stochastic microstructure modeling*

Introduction

It is widely accepted that the 3D microstructure of porous and composite materials has a strong influence on effective transport processes in these materials, e.g. on electric and ionic conductivities in solar cells, fuel cells and batteries. In order to perform materials optimization in a reliable and efficient way, it is necessary to understand the relationship between microstructure and effective transport properties on a quantitative level. The question that we address here is how the complex geometry of a microstructure influences conductive transport processes. Several formulas exist in the literature suggesting that volume fraction of the transport phase (ε), windedness of transport pathways (tortuosity τ) and bottlenecks (constrictivity β) play a major role.[1–7]

Recently, Gaiselmann et al.[8] have proposed a general relationship between geometric characteristics and effective conductivities of the following type: $\sigma_{\text{eff}} = \sigma_0 a \frac{\varepsilon^b \beta^c}{\tau^d}$ for certain parameters $a, b, c, d \geq 0$ and intrinsic conductivity σ_0. To get suitable values of these parameters, 44 virtual 3D microstructures generated by a random graph model were analyzed. For each microstructure, geometric characteristics (volume, constrictivity, geometric tortuosity) and the effective conductivity σ_{eff} (using the finite element method) were determined. Error-minimization led to the following expression: $\sigma_{\text{eff}} = \sigma_0 2.03 \frac{\varepsilon^{1.57} \beta^{0.72}}{\tau^2}$. Their approach - combining stochastic microstructure modeling with finite element simulations - was referred to as *virtual materials testing* (VMT).

In the older literature[2,3,6] the micro-macro relationships are usually described by a similar type of equation as it is proposed by Gaiselmann et al.[8]

However, the older investigations came up with simple integral numbers for the parameters (usually 1 or 2, positive or negative). A typical example is the influence of path length (i.e. tortuosity). Based on theoretical considerations it was argued that tortuosity should carry the exponent -2 (i.e. τ^{-2}). In Gaiselmann et al.[8] the parameters are determined based on a statistical error minimization procedure, and using empirical data from VMT. It is important to note that the result of such a statistical approach strongly depends on the methods used to access the empirical data. For example the resulting parameter values depend on the image processing technique used to determine tortuosity. As a consequence of the statistical approach the parameters tend to be non-integer numbers, and only accidentally simple integers are obtained.

In the present paper, we extend the study performed by Gaiselmann et al.[8] in several ways. The goal is to establish empirical relationships between effective transport properties and geometric characteristics using the same virtual microstructures, but also to critically analyze and evaluate the methodologies used to determine the microstructure characteristics, which are the following:

Tortuosity. In a simplified way, tortuosity $\tau \geq 1$ can be described as the mean shortest transport path length divided by the sample thickness. It is a measure for the windedness of transport paths. There are various definitions of tortuosity used in geology, physics, engineering and image analysis. We analyze the sensitivity of the predictive formulas depending on which type of tortuosity is considered. By comparing two types of tortuosity, geometric tortuosity τ_{geom} and geodesic tortuosity τ_{geod}, it will be shown in this paper that the choice of tortuosity has a significant impact on the predictive formulas.

Constrictivity. Constrictivity $\beta \in [0, 1]$ is a measure for the strength of bottleneck effects. Constrictivity was introduced by E. E. Petersen[9] for flow in simple pipes. It was shown that the influence of hyperbolic constrictions on the

flow properties in pipes scales with the ratio of the minimum cross sectional area over the maximum cross sectional area. This leads to the following expression: $\beta = \frac{\pi r_{\min}^2}{\pi r_{\max}^2} = \left(\frac{r_{\min}}{r_{\max}}\right)^2$. For disordered microstructures this concept was difficult to apply, since minimum and maximum cross sections are difficult to access. However, with the progress in tomography and 3D image analysis new methods became available to describe different characteristics of size distributions in complex microstructures. For example Münch and Holzer[10] presented a method to describe the size distribution of bulges in continuously networked microstructures, which was called continuous pore size distribution (c-PSD). It is applicable to both particle and pore networks. In the same paper it is also shown that mercury intrusion porosimetry (MIP) is a suitable method to capture bottleneck sizes.[11] The MIP-PSD curves usually show a steep decrease of cumulated volume (y-axis) within a narrow range of pore sizes (x-axis). This steep decrease in volume is interpreted as the so-called breakthrough of the intruding liquid and the narrow range of sizes is therefore considered as characteristic dimensions of the bottlenecks. In addition to the experimental porosimetry, MIP-PSDs can also be determined with numerical simulations, using tomographic data as input. In this way the typical bottleneck dimensions can also be accessed for solid phases. Hence with these 3D methods the size distributions of bulges and bottlenecks can now be accessed for a wide range of materials and the study of various transport properties. Furthermore, in this way the concept of β as $\beta = (r_{\min}/r_{\max})^2$ can now be applied also to complex disordered microstructures, as shown by Holzer et al.[5] Thereby, the average size of bulges ($r_{\max}$) was defined as the radius corresponding to the 50% quantile of the c-PSD curve. In analogy, the average size of bottlenecks ($r_{\min}$) is defined as 50% quantile of the MIP-PSD curve. It should be noted that this definition (i.e. using the 50% quantile) is reasonable but somewhat arbitrary. Thus, in the present study we also address

the question if there are better definitions for constrictivity. Why using 50% quantiles and does one really need both characteristics, MIP-PSD and c-PSD to describe the bottleneck effect? Why not define constrictivity in a different way? To answer these questions, we consider various definitions of constrictivity and analyze their capability to predict effective transport properties.

Volume fraction. The third microstructure characteristic is volume fraction $\varepsilon \in [0, 1]$ of the transport phase. For example, the electrical conductivity in composite solid oxid fuel cell (SOFC) anodes strongly depends on the nickel content. Of course, it is only the connected portion of this phase which contributes to the transport. Thus it is more correct to consider only the connected portion, which is then the effective volume fraction (ε_{eff}). Nevertheless, in the present work we are dealing with virtual microstructures from stochastic simulation, which are based on a fully connected random graph model.[8] Therefore, in this paper the volume fraction is per definition identical with the effective volume fraction (i.e. 100% percolating). It must be emphasized that the virtual microstructures used in this work are identical with those from Gaiselmann et al.[8] (minus one structure with extreme properties). However, in this work we address some important questions about the underlying concept, and we use some refined methodologies to increase reliability and precision of predictions. For example, we compute the effective conductivities directly on the voxel-grid obtained from tomography using GeoDict[12] instead of using a reduced, triangulated mesh as input for the finite elment method (FEM). Thus, we omit the uncertainty introduced by the meshing of the voxel-grid as in Gaiselmann et al.[8] As a consequence, the computed effective conductivies slightly change. This also results in different values of parameters of the fitting.

Furthermore, we extend the study of Gaiselmann et al.[8] by differentiating between *training errors* and *prediction errors*.[13] If predictive capability of the

established relationships is of major interest, then the prediction error should be considered, as it is done in the present study.

This paper is organized as follows. To begin with, we present the data basis from VMT with the corresponding geometric characteristics (volume fraction, constrictivity, tortuosity) and the transport processes. Then, the statistical methods are introduced, before prediction of effective conductivity is discussed. Moreover, geometric and geodesic tortuosities are compared and various definitions of constrictivities are analyzed. Finally, we propose a quantitative relationship between microstructure characteristics and effective conductivity, which is validated with experimental data.

Data & Methods

Data Basis: 3D Microstructures

In total, 43 microstructures with different volume fractions (ε), windedness of transport paths (tortuosity τ) and bottlenecks (constrictivity β) have been generated using a stochastic microstructure model, see Figure 1. The model has been introduced by Gaiselmann et al.[8] and provides an excellent data basis to investigate empirically the relationship between geometric characteristics and effective transport properties. In general, the stochastic microstructure model uses tools from stochastic geometry (e.g. point processes, random graphs) and generates random 3D geometries that can be interpreted as microstructures. The stochastic model can generate a large variety of different microstructures. The variability of simulated microstructures is illustrated in Figure 1. The example on the left has intermediate properties, in terms of ε, β and τ. The middle example has a strong anisotropy, which leads to a high tortuosity ($\tau \gg 1$) for the vertical transport direction. The example on the right side is character-

ized by relatively large bulges ($r_{\max}$) and small bottlenecks ($r_{\min}$), which results in a small constrictivity value ($\beta \ll 1$). The analyzed 43 microstructures cover a wide range of values for volume fraction ($\varepsilon \in [0.15, 0.55]$), constrictivity ($\beta \in [0.04, 0.61]$) and geodesic tortuosity ($\tau_{\text{geod}} \in [1.10, 2.74]$), see also Figure 2. The large variation of microstructure characteristics is difficult to cover with an experimental approach (e.g. by fabrication of real samples with powder processing and sintering). A disadvantage of the virtual approach, however, is the fact that the effective properties can not be measured experimentally. For this aspect we rely on numerical transport simulations.

Geometric Characteristics

The goal of this study is to quantify microstructure effects. It is important to note that the values of the measured characteristics τ, β and ε strongly depend on the image analysis methods and on the underlying geometrical concepts. The applied methods for these characteristics are briefly explained in the following.

There exist several different definitions and different measurement techniques for tortuosity.[4] To quantify the effect of the windedness of transport paths, we consider two types of tortuosities: geodesic tortuosity (τ_{geod}) and geometric tortuosity (τ_{geom}).

For the geodesic tortuosity the shortest path lengths (in terms of geodesic distance[14]) in transport direction from inlet- to outlet-planes are calculated within the voxel space that represents the transporting phase (see Figure 3 left). Geodesic tortuosity τ_{geod} is then defined as the ratio of geodesic distance over material thickness ℓ. To obtain a statistically solid estimate of τ_{geod}, we consider an average of geodesic tortuosities computed for all voxels of the transporting phase in the inlet-plane. Geometric tortuosity is similar to geodesic tortuosity, but the shortest paths are calculated on a skeleton of the transporting phase,

see Figure 3 (center and right). For the calculation of the skeleton, we used Avizo 7.[15] The shortest paths are calculated using the Dijkstra algorithm.[16] Geodesic tortuosity is computed in the same way as geometric tortuosity if the transporting phase of the microstructure is interpreted as a graph where each voxel is a node and all neighboring voxels (with respect to the 26-neighborhood) are connected. Note that geometric tortuosity is typically larger than geodesic tortuosity as the shortest paths for geometric tortuosity are restricted to a graph, which is a subset of the transporting material phase. For the 43 microstructures, an empirical relationship of $\tau_{\mathrm{geod}} = 0.76\tau_{\mathrm{geom}}$ is obtained by linear regression where the intercept is set to zero ($R^2 = 0.81$).

The effect of bottlenecks (narrow throats) is measured in terms of constrictivity β defined as $\beta = \left(\frac{r_{\mathrm{min}}}{r_{\mathrm{max}}}\right)^2$, see Holzer et al.[5] Thereby, speaking heuristically, r_{min} indicates the radius of the typical bottleneck and r_{max} the radius of the typical bulge, see Figure 4 (left). To compute r_{min} and r_{max} from a 3D microstructure, the concept of the continuous pore size distribution (c-PSD) and the computational mercury-intrusion-porosimetry pore size distribution (MIP-PSD), which allow the simulation of MIP, are needed, see Münch and Holzer.[10]

The c-PSD $P(r)$ is the volume fraction of the phase of interest, which can be covered by spheres with radius r where the spheres have to be completely located in this phase, see Figure 5 (left). The parameter r_{max} is the radius such that 50% of the phase volume can be covered by spheres with this radius. Mathematically speaking, $r_{\mathrm{max}} = P^{-1}(0.5)$ with P^{-1} being the quantile function of P, see also Figure 4 (right).

The concept of the MIP-PSD is leaned on the MIP (mercury intrusion porosimetry): MIP is an experimental technique to characterize the pore-size distribution in porous materials. The MIP measurements are strongly influenced by narrow constrictions along the intrusion pathways.

The basic idea for the simulation of MIP-PSD is to consider a 'directed filling' of the phase of interest by spheres. More precisely, those regions of the phase of interest are filled which can be reached by a sphere with radius r, starting from the inlet plane of the material, see Figure 5 (right). Thereby, the spheres are restricted to be located completely in the phase of interest. The volume fraction of these regions for a certain radius r is denoted by $mP(r)$. Typically, the curve of $mP(r)$ exhibits a significant decrease for radii larger than a certain value, see Figure 4 (right). This radius, which is also called 'breakthrough radius', is considered as being equivalent with the characteristic size of the bottlenecks. The parameter $r_{\min}$ is defined by $r_{\min} = mP^{-1}(0.5)$, i.e. the 50% quantile. For further information about the c-PSD, MIP-PSD, and constrictivity β, the reader is referred to Holzer et al. and Münch and Holzer.[5,10] In the Section 'Testing Different Definitions of Constrictivity', we will analyze more carefully if this definition describes the effect of bottlenecks in a meaningful way. In the following, we denote the constrictivity as $\beta = \left(\frac{r_{\min 50}}{r_{\max 50}}\right)^2$ in order to emphasize the use of the 50% quantiles.

The volume fraction ε is defined as the ratio of the volume of the transporting phase divided by the total volume of the 3D image and can be estimated simply by counting voxels. As mentioned earlier all virtual microstructures used in this study are based on a fully connected graph model. Hence, throughout this paper ε represents the volume fraction of the entire connected phase.

Transport Processes

As in Gaiselmann et al.[8], we consider conductive transport processes within composite or porous materials, where only one phase is conducting. The electric

charge transport is described by Ohm's law

$$J = -\sigma \frac{dU}{dx} \tag{1}$$

and

$$\frac{dU}{dt} = \sigma \frac{d^2U}{dx^2} \tag{2}$$

where J is the current density, σ is the conductivity, U is the electric potential, and t is time. With constant boundary conditions, such systems converge to a steady state which is described by the Laplace equation

$$\frac{d^2U}{dx^2} + \frac{d^2U}{dy^2} + \frac{d^2U}{dz^2} = 0, \tag{3}$$

where x, y, and z denote the spatial coordinates.

Since transport only takes place in one phase, the geometry of the microstructure influences the effective conductivity σ_{eff} as follows:

$$\sigma_{\text{eff}} = \sigma_0 M. \tag{4}$$

Thereby, σ_0 is the intrinsic conductivity (i.e., without geometric constraints), and M is a reduction factor, where all the transport limitations caused by geometry of the microstructure are included.

The goal is to predict the $M-$factor on the basis of the geometric characteristics ε, τ, β, i.e. we are a looking for a relationship of the type $M = f(\varepsilon, \beta, \tau)$.

For each of the 43 synthetic microstructures, the effective conductivity and the associated M-factor (M_{sim}) are simulated using the software GeoDict.[12]

Statistical Methods

Using statistical methods we aim to find an empirical relationship between the microstructure characteristics $(\varepsilon, \beta, \tau)$ and the M-factor (M_{predict}), so that this relationship can be used to predict the effective conductivity for any 3D microstructure (e.g. using tomography). For this purpose the predictive capability of 12 different equations describing the relationships between geometric characteristics and M-factors (e.g. $M = \frac{\varepsilon\beta}{\tau^2}$) are analyzed with statistical methods (see Table 1). Thereby we consider the relative error in percent between predicted and simulated M-factors, which is given by the so-called $MAPE$ (mean absolute percentage error) with

$$MAPE(\vec{M}_{\text{sim}}, \vec{M}_{\text{predict}}) = \frac{1}{n} \sum_{i=1}^{n} \frac{|M_{\text{sim},i} - M_{\text{predict},i}|}{M_{\text{sim},i}} \cdot 100\%. \tag{5}$$

Thereby, $\vec{M}_{\text{sim}} = (M_{\text{sim},1}, \ldots, M_{\text{sim},n})$ (from GeoDict[12]) is a vector of simulated M-factors for n microstructures and $\vec{M}_{\text{predict}} = (M_{\text{predict},1}, \ldots, M_{\text{predict},n})$ a vector of predicted M-factors. The $MAPE$ indicates the error made by the predictions. A lower $MAPE$ indicates a higher predictive capability.

In Gaiselmann et al.,[8] a general relationship of the following form has been proposed:

$$M = \frac{a\varepsilon^b \beta^c}{\tau^d} \tag{6}$$

for suitably chosen values of the parameters $a, b, c, d \in [0, \infty)$. Many well-known relationships are included as specific examples, e.g. Archie's law[1] $M = \varepsilon^b$ can be obtained by choosing $a = 1$ and $c = d = 0$.

The values of the parameters in the above formula are chosen to minimize the mean absolute percentage error ($MAPE$), where the optimization is carried out using simulated annealing which is a stochastic optimization algorithm.[17]

When formulas are fitted to data, it is important to distinguish between

training errors and prediction errors.[13] Fitting a formula to data means that the parameters are 'trained'. If the error is computed for the same data that was used for fitting, then this is called *training error*. When the error is computed for new, unseen data that have not been used for fitting, it is called *prediction error*. Differentiating between training errors and prediction errors is crucial in order to avoid overfitting.[13] Imagine we would have a formula not with four parameters a, b, c, d, but with, say, 30 parameters. Then fitting the formula with 30 parameters to the data with 43 samples would probably yield an extremely small training error. But it is very likely that the formula is fitted too much to the specific details of the data such that the fitted formula does not capture the general relationships any more. Thus, the error for new, unseen data (prediction error) might be rather large. Typically, with increasing number of (model) parameters, the training error decreases. The prediction error first decreases as well and then increases again when model complexity (i.e. number of parameters) exceeds a certain threshold.

The prediction error is estimated by K-fold cross-validation with $K = 7$.[13] The idea is to split the data set into K parts $1, \ldots, K$ of (more or less) equal size. For $k = 1, \ldots, K$, the kth part is used as test data and the remaining $(K - 1)$ parts are used as training data. The formula is then fitted to the training data and the error is computed for the test data. This yields K fittings of the formula and K test errors. The average of the test errors is an estimate for the prediction error. For statistical accuracy, we repeated the K-fold cross-validation 80 times with using randomly permuted data sets. The training error is computed using the averaged parameters from repeated fittings of the formula. The results are displayed in Table 1.

Results & Discussion

In this paper, we aim to establish a formula that predicts the microstructure influence on effective transport properties (here: conductive transport) on the basis of geometrical characteristics (volume fraction ε, constrictivity β, tortuosity τ). In addition, we analyze the sensitivity of the predictive formulas depending on which type of tortuosity is being considered. Finally, we analyze how well the established definition of constrictivity β describes the effect of bottlenecks. To answer this question, we consider a total of 35 different constrictivity definitions and analyze their capability to predict effective transport properties.

Predicting the Microstructure Influence on Effective Conductivity (M-factor)

Table 1 shows 12 different equations that are tested for their predictive capabilities using statistical methods. All 12 equations are derived from the following basic equation: $M = \frac{a\varepsilon^b\beta^c}{\tau^d}$ by varying the values of the parameters a, b, c, d. For example the well-known relationship of eq. (9) $M = \frac{\varepsilon\beta}{\tau^2}$ is obtained with $a = b = 1, c = 0$ and $d = 2$. In principle one can distinguish 4 subgroups of the investigated equations. The first group (eqs. (7)-(9)) represents standard equations, that have been widely used in literature since a long time.[1–3] From eqs. (7) to (9) more microstructure characteristics are introduced step by step. The equations of the second group (eqs. (10)-(12)) have a similar structure, but fitted values of parameters b, c, d are introduced, so that eqs. (8),(11) as well as (9),(12) can be read as related couples. The equations of the third group (eqs. (13)-(16)) then contain an additional prefactor a. In this way, eqs. (8),(11),(15) and (9),(12),(16) become related triples with a similar structure. The last two eqs. (17) and (18) are special cases with both fitted parameters and fixed integers as exponents.

The 'standard' equations and the importance of fitting. Regarding the first group with traditional equations (eqs. (7)-(9)), it should be noted that eqs. (8) and (9) have fixed integers as parameters b, c, d, which are derived from theoretical considerations. In contrast, Archie's law (eq. (7)) was applied in geological studies by fitting the exponent b for experimental data. Probably the most frequently used equation is eq. (8), which includes volume fraction and tortuosity. In our analysis it has the highest prediction error. In comparison, eq. (7) has a much lower error, although it considers only volume fraction as geometric characteristic. The improvement compared to eq. (8) is attributed to the involved fitting procedure. Also eq. (9) has a lower error compared to eq. (8), although it includes no fitting of parameters. This improvement can be attributed to the fact that eq. (9) considers all three microstructure characteristics, including constrictivity. Hence, already the analysis of the first three (traditional) equations gives evidence that both, looking at all 3 characteristics and performing a fitting procedure, contribute to better predictions. Consequently, applying fitting procedures to eq. (9), which considers all three characteristics, will lead to a further reduction of prediction errors as shown for eqs. (12) and (16)-(18). It is plausible that fitting of the parameters improves the predictive capability significantly. First, the parameters are fitted such that they predict a certain output (here: effective conductivities or M-factors). But also, since tortuosity and constrictivity are defined as volume averaged characteristics from disordered 3D structures, one cannot expect that simple integers (e.g. ε^1 or τ^2) will describe accurately their relationship with the effective physical properties.

Eq. (8) plays a special role, since it is often used for implicit tortuosity calculations, instead of measuring tortuosity from tomography using image analysis. The procedure for implicit tortuosity measurement is as follows: if the microstructure influence (M-factor) and the volume fraction are known, then

solving eq. (8) for τ yields $\tau_{\text{eq.2}} = \sqrt{\frac{\varepsilon}{M}}$). It should be noted that this kind of implicit tortuosity does not carry real geometric information of the pathways' lengths. To describe the microstructure effect well, all three characteristics ε, β and τ are required. Using eq. (9), for example, would yield $\tau_{\text{eq.3}} = \sqrt{\frac{\varepsilon\beta}{M}}$. Thus, determining tortuosity by $\tau_{\text{eq.2}} = \sqrt{\frac{\varepsilon}{M}}$ leads to a characteristic that describes the effect of tortuous pathways *combined* with the bottleneck effect since $\tau_{\text{eq.2}} = \frac{\tau_{\text{eq.3}}}{\sqrt{\beta}}$. This shows that if tortuosity is computed by $\tau_{\text{eq.2}} = \sqrt{\frac{\varepsilon}{M}}$, one needs to be careful about the interpretation.

Necessity of all characteristics ε, β, τ. In accordance with Gaiselmann et al.,[8] it can be seen that all parameters ε, β, τ are required to describe the influence of the microstructure on conductive transport processes. Using only volume fraction ε (eq. (7), Archie's law) yields a relatively high prediction error of 37.96%. Considering volume fraction ε and either constrictivity β (eq. (10)) or geodesic tortuosity τ_{geodesic} (eq. (11)) lowers the prediction error to 36.54% and 25.43%, respectively. Taking all three characteristics into account (eq. (12)) yields a prediction error of 19.06% (using geodesic tortuosity).

At this stage it must be emphasized that the fitting procedure was performed always for geodesic as well as for geometric tortuosity (see Table 1). The differences between results obtained by using geodesic and geometric tortuosities will be discussed below.

The 'best' equation. At this stage, the question is still open which equation is 'best'. One might argue that the 'best' equation is eq. (16) using geometric tortuosity since it offers the overall lowest prediction error. However, it should be taken into account that the prefactor of 2.08 could lead to effective conductivities *larger* than the intrinsic conductivity when the constraint of the microstructure is very small, e.g. $\varepsilon = 0.9, \beta = 0.9, \tau_{\text{geom}} = 1.1$. Gaiselmann et al.[8] therefore suggested to limit the predicted M-factor to 1, e.g.

$M_{\text{predict}} = \min\left(1, 2.08\frac{\varepsilon^{1.62}\beta^{0.49}}{\tau_{\tau_{\text{geod}}}^{2.26}}\right)$. In this case, two microstructures with identical volume fractions (e.g. 0.9), constrictivities (e.g. 0.9) but different tortuosities (e.g. 1.1 and 1.2) would be assigned the same M-factor of 1, i.e., the two microstructures would have the same effective conductivities, although the microstructure with tortuosity of 1.2 should have a smaller effective conductivity.

For this reason we prefer equations (12) and (17) (with prediction errors of 19.06% and 17.69%) using geodesic tortuosity. These equations are most suitable to predict the M-factor and the associated effective conductivity in a reliable way.

Geometric Tortuosity vs. Geodesic Tortuosity

Tortuosity is widely used in the research community, but there exists no unique definition of this notion.[4] In this paper, we consider two types of tortuosities both of which are geometry-based: geometric tortuosity τ_{geom} and geodesic tortuosity τ_{geod}. Comparing the values of the two tortuosities for all 43 virtual microstructures indicates an almost linear relationship. Linear regression with intercept 0 results in $\tau_{\text{geod}} = 0.76\tau_{\text{geom}}$. However, the results in Table 1 also indicate that there are some fundamental differences between the geometric and geodesic cases. Therefore, in this section we investigate whether and how the type of tortuosity has an influence on the predictive capability of empirically fitted formulas.

Importance of calibration. First, note that the parameters b, c, d in the fitted formulas (e.g. eqs. (11)-(12)) deviate significantly when using geometric or geodesic tortuosity. In eq. (12), for example, the exponent for the geodesic tortuosity is three times larger than for the geometric tortuosity. Interestingly, the lowest prediction errors using either geometric or geodesic tortuosity are very similar: 17.69% (eq. (17), geodesic tortuosity) and 17.24% (eq. (16),

geometric tortuosity). Two conclusions can be drawn from this: First, it is absolutely essential to fit the formulas depending on what type of tortuosity has been used. Second, the choice of tortuosity has a significant impact on the fitted parameters and on the corresponding prediction errors. This shows how important it is to be precise with the definition of tortuosity.

The role of the prefactor a. Choosing a different type of tortuosity also has a strong impact on the prefactor a, which is briefly discussed in this section. Basically eqs. (13)-(16) (with prefactors $a \neq 1$) can be considered as analogous to equations (7), (10)-(12) (where $a = 1$). The comparison of these two sets of analogous equations shows that the training error decreases, as expected, when the prefactor is introduced. In the geodesic case, however, the difference for the training error is not large. Furthermore considering the prediction errors, for eqs. (13),(14) compared to (7),(10) the values even slightly increase, which might indicate a slight overfitting. For eqs. (15),(16) compared to (11),(12), the prediction errors are nearly identical for the geodesic case. In contrast, for the geometric case the introduction of a prefactor (eqs. (15),(16)) leads to a significant reduction of the errors (compared to eqs. (11),(12)). One possible explanation is that this prefactor aims to systematically decrease the value of geometric tortuosity (cf. eq. (16)): $\frac{2.08\varepsilon^{1.62}\beta^{0.49}}{\tau_{\mathrm{geom}}^{2.26}} = \frac{\varepsilon^{1.62}\beta^{0.49}}{(0.72\tau_{\mathrm{geom}})^{2.26}}$. Thus, introducing the prefactor of 2.08 is equivalent to decreasing τ_{geom} to $0.72\tau_{\mathrm{geom}}$. For eq. (15), applying the same procedure, introducing the prefactor of 1.82 is equivalent to decreasing τ_{geom} to $0.74\tau_{\mathrm{geom}}$. These relationships derived from the fitted formulas are very similar to the above-mentioned linear regression, which is given by $\tau_{\mathrm{geod}} = 0.76\tau_{\mathrm{geom}}$. Interestingly, for the geodesic case in eqs. (15)-(16), the fitted prefactors are close to one (i.e. 0.87, 0.88) and the prediction error is similar to the case of a constant prefactor equal to 1 (eqs. (11)-(12)). Thus, with the geodesic tortuosity, there appears to be no need to re-scale the

values of the tortuosity. Concluding, there is empirical evidence that geometric tortuosity overestimates the windedness of transport paths - with respect to conductive transport processes. Consequently, geodesic tortuosity is capturing the windedness of transport paths with respect to conductive transport processes more adequately.

Testing Different Definitions of Constrictivity

The constrictivity β is defined by $\beta = (r_{\min 50}/r_{\max 50})^2$, where $r_{\min 50}$ and $r_{\max 50}$ are the 50%-quantiles of the MIP-PSD and c-PSD, respectively. Why not defining constrictivity differently, e.g. $\beta = (r_{\min 90}/r_{\max 10})^2$? In the following, we test a series of potential constrictivity definitions using different quantiles of c-PSD and MIP-PSD. In particular, we distinguish three types of constrictivity candidates, where the definition is based

1. solely on quantiles of the c-PSD, e.g. $\beta = (r_{\max 75}/r_{\max 50})^2$,
2. solely on quantiles of the MIP-PSD, e.g. $\beta = (r_{\min 90}/r_{\min 10})^2$,
3. on quantiles of c-PSD and MIP-PSD, e.g. $\beta = (r_{\min 90}/r_{\max 75})^2$.

The first case can be considered as a constrictivity which only depends on the more traditional size distribution of the bulges (c-PSD). In the second case constrictivity is entirely related to variations of the bottleneck-dimensions (MIP-PSD). The third case finally considers relationships between the sizes of bulges and bottlenecks.

Note that the constrictivity must be between 0 and 1. This puts a constraint on which constrictivity candidates are admissible. For example, $\beta = (r_{\max 25}/r_{\max 50})^2$ yields values greater than one and is consequently inadmissible.

Let's look at the study in more detail. For all 43 microstructures, we computed the $10\%, 25\%, 50\%, 75\%$ and 90% quantiles of the c-PSD and MIP-PSD. Subsequently, we consider all admissible definitions of β, i.e., ensuring that $\beta \in [0, 1]$. We then fit selected equations (eqs. (9),(12),(16),(17),(18)) using 35 admissible definitions of constrictivity and compute the prediction errors either using geometric or geodesic tortuosity. This yields a total of 350 prediction errors (5 equations, 35 constrictivity candidates, 2 types of tortuosity). To analyze this enormous data, we state the constrictivity candidates in each of the three classes (c-PSD, MIP-PSD, both) with the lowest prediction error for the individual equations. Thereby, the prediction errors are averaged over geometric and geodesic tortuosity. The results are given in Table 2. First, note the results slightly change compared to Table 1 which is due to the randomness of the optimization algorithm used for fitting the formulas. An important finding is that there is no definition of constrictivity that is 'best' (i.e., lowest prediction error) regarding all equations. However, the constrictivities based on both, MIP-PSD and c-PSD always outperform those based on either c-PSD or MIP-PSD. Thus, to accurately describe the bottleneck effect, both, MIP-PSD and c-PSD, are required. Also note that for each equation, the prediction errors using the established constrictivity definition (using the 50%-quantiles of c-PSD and MIP-PSD, respectively) are very close to the lowest prediction errors. In short, the established constrictivity definition performs well in all situations. This suggests that $\beta = (r_{\mathrm{min}50}/r_{\mathrm{max}50})^2$ describes the effect of bottlenecks quite well.

So, which constrictivity candidate will give the best *overall* prediction accuracy, i.e. if the prediction errors are averaged over all five equations. These results are given in the last row of Table 2. The data suggests that constrictivity based on the 25%-quantiles of MIP-PSD and c-PSD describes the effect of

bottlenecks best. However, the difference in terms of average prediction error is extremely close to the established definition (24.85% vs. 26.49%). In addition, the established definition of constrictivity has the second lowest overall prediction error among the 35 constrictivity candidates. To decide which definition is best is a difficult task - also due to the nature of stochastics: imagine you could try 10000 definitions of constrictivity and test them on 43 samples. Then probably, there will be one definition with an extremely low prediction error. But is this definition really performing best or is it just by chance? To give a statistically solid answer on which constrictivity definition is best, one would require more data. From our point of view two statements can be made: First, constrictivity requires both, c-PSD and MIP-PSD. Second, the established constrictivity definition describes the effect of bottlenecks quite well.

Validation with Experimental Microstructures

Results from two recent publications are used to validate the above proposed relationship (eq. (12)) between the effective transport properties (σ_{eff} or D_{eff}) and the microstructure characteristics (ε, β and τ). These literature data include six different SOFC anodes (details can be found in Pecho et al.[18]), as well as four different porous membranes used as liquid junctions in pH-sensors.[19] Both studies provide 3D data acquired with FIB-tomography and subsequent 3D-analyses, that were performed with the same methods used in this paper (i.e. the same image processing algorithms were applied for measuring ε, β and τ). Furthermore, also the same numerical transport simulations with GeoDict were applied to compute the effective transport properties (i.e. effective conductivity in solid phases and effective gas diffusivity in pores) by using tomography data as morphological input. By substituting the measured values for ε, β and τ into eq. (12) the so-called predicted M-factor (M_{pred}) is obtained. In order to test

reliability and precision of the proposed method, M_{pred} is compared with an independent M-factor from simulation. This so-called M_{sim} is defined as the ratio of the effective transport property (σ_{eff} or D_{eff}, resulting from numerical transport simulation) over the intrinsic transport property (σ_0 or D_0, used as input for the simulation). It must be emphasized that numerical simulations with GeoDict are capable to capture the microstructure influence on the effective conductivity, diffusivity and permeability in a reliable and precise way. This capability was proven by comparison with experimental measurements (see e.g. Becker et al.[20]). Consequently we consider M_{sim} as a suitable reference to test reliability and precision of eq. (12) for predicting M_{pred} and the corresponding effective properties (conductivity or diffusivity), respectively. The data from literature used for validation are shown in Figure 6. They include 16 data points, which are grouped into the following three subsets: a) White rhombs represent properties of the nickel-phase in six different SOFC-anodes (related to effective electrical conductivity). b) Gray squares represent properties of yttria-stabilized Zr-oxide (YSZ) in the same six SOFC anodes (related to effective ionic conductivity). c) Black triangles describe the properties related to effective gas diffusivity in porous membranes for sensor applications. In Figure 6 (A) the data points are nicely located along the reference line, where M_{sim} is equal to M_{pred}. These results thus confirm the capability of eq. (12) to predict the effective transport properties based solely on microstructure characteristics. Two data points (white rhombs) for nickel in medium- and in coarse-grained anodes exhibit unusually high values for M_{sim} as compared to the corresponding M_{pred}. It was shown that these two samples underwent severe nickel-agglomeration due to the exposition to harsh operating conditions including repeated redox-cycling at 950°C.[18] It was furthermore documented that the nickel-agglomeration also led to an increase of the representative elementary volume (REV), which clearly

exceeds the size of the image window covered with FIB-tomography. The offset of these two data points can be explained by the lack of representativeness in the underlying 3D-analyses. The offset is thus not due to an eventual inaccuracy of the prediction methods involving eq. (12).

The quality of such a validation is also dependent on the range of microstructure characteristics, which is covered by the underlying data. As shown in Figure 6 (B-E), the data from literature cover a reasonably wide range ($\varepsilon : 0.03 - 0.4, \beta : 0.01 - 0.48$ and $\tau : 1.1 - 1.9$). These plots also document that no general correlation between ε, β and τ can be observed. For example the data do not obey the Bruggemann-correlation (i.e. $\tau = \varepsilon^{-0.5}$), which is frequently postulated in literature. This indicates that there is reasonable randomness and variability in the parameter-constellations of our data basis, which is also strengthening the quality of this validation. In summary, the literature data reveal a good match between M_{pred} and M_{sim}, which supports a high prediction capability of eq. (12). A very similar result is also obtained for eq. (11) (not shown). The $MAPE$ is 23.3 % (excluding the two outliers). Hence, the $MAPE$ for these literature data with real microstructures is very similar to the $MAPE$ calculated earlier in this study for virtual microstructures (i.e. 22.4%, see Table 2).

Conclusions

In the present paper, we analyzed how the complex geometry of a disordered microstructure influences conductive transport processes. Therefore, we considered 43 synthetic microstructures that were generated by a stochastic model. For each microstructure, geometric characteristics (volume, constrictivity, tortuosity) and the effective conductivity σ_{eff} (using FEM) have been determined.

As in Gaiselmann et al.,[8] to establish a link between geometric characteristics

and effective conductivities, a formula of the following type was considered: $\sigma_{\text{eff}} = \sigma_0 a \frac{\varepsilon^b \beta^c}{\tau^d}$ for some parameters $a, b, c, d \geq 0$ and intrinsic conductivity σ_0. Error-minimization led to the following expressions: $\sigma_{\text{eff}} = \sigma_0 \frac{\varepsilon^{1.15} \beta^{0.37}}{\tau^{4.39}}$ (prediction error 19.06%) or $\sigma_{\text{eff}} = \sigma_0 \frac{\varepsilon \beta^{0.36}}{\tau^{5.17}}$ (prediction error 17.69%). It was shown that all three characteristics ε, β, τ are required in order to describe the influence of the microstructure on the effective conductivity in a reliable and accurate way.

Besides the predictive formulas, we wanted to have a closer look at the choice of the geometric characteristics, in particular tortuosity and constrictivity.

A comparison between geometric and geodesic tortuosity revealed that geometric tortuosity tends to overestimate the effect of tortuous pathways with respect to conductive transport processes. But more importantly, it was shown that it does make a significant difference which type of tortuosity is used.

Finally, we wanted to analyze how well the established definition of constrictivity describes the effect of bottlenecks. Therefore, we performed a simulation study where we estimated the relative prediction error for various definitions of constrictivity. We found that the established constrictivity definition based on $50\%-$quantiles of the continuous pore size distribution (c-PSD) and the computational mercury-intrusion-porosimetry pore size distribution (MIP-PSD) describes the effect of bottlenecks extremely well for all considered situations. In addition, describing the bottleneck effect sufficiently well requires both characteristics, c-PSD and MIP-PSD.

The empirical relationship described in this study is of general meaning regarding microstructure effects. It can be used to predict conductivity for different kinds of materials. It also introduces the quantitative basis, which is necessary to perform knowledge-based materials optimization. In the future it will also serve as the basis for an improved understanding of microstructure

degradation on a quantitative level in all kinds of materials (e.g. porous electrodes in fuel cells, batteries etc).

Acknowledgements

The authors kindly acknowledge financial support from the following institutions: SNSF grant Nr 407040_154047 (Smart materials concepts for SOFC anodes), SNSF grant Nr 407040_153790 (Designing multifunctional materials for PEM fuel cells), SWISS CTI grant Nr 16851.1 PFNM-NM (Nanoporous diaphragms for electrochemical sensors - NanoDiaS). O. Pecho was supported by SNSF grant Nr 200021_135270 (Relationships between 3D topology and SOFC electrode performance). We kindly thank Gerd Gaiselmann for providing the 43 microstructure samples used in this paper.

References

[1] Archie GE. The electrical resistivity log as an aid in determining some reservoir characteristics. Trans Am Inst Mining Metallurg Pet Eng. 1942;146(1):54–61.

[2] Brakel JV, Heertjes PM. Analysis of diffusion in macroporous media in terms of a porosity, a tortuosity and a constrictivity factor. Int J Heat Mass Transf. 1974;17(9):1093–1103.

[3] Carman PC. Flow of Gases through Porous Media. New York: Academic Press, 1956.

[4] Clennell MB. Tortuosity: A guide through the maze. In: Lovell MA, Harvey PK, eds. Developments in Petrophysics. London: Geological Society Special Publications, 1997;299–344.

[5] Holzer L, Wiedenmann D, Muench B, Keller L, Prestat M, Gasser P, Robertson I, Grobéty B. The influence of constrictivity on the effective transport properties of porous layers in electrolysis and fuel cells. J Mater Sci. 2012;48(7):2934–2952.

[6] Kozeny J. Ueber kapillare Leitung des Wassers im Boden. Sitzungsber Akad Math Naturwiss. 1927;136a:271–306.

[7] Wiedenmann D, Keller L, Holzer L, Stojadinovic J, Münch B, Suarez L, Fumey B, Hagendorfer H, Brönnimann R, Modregger P, Gorbar M, Vogt UF, Züttel A, Mantia FL, Wepf R, Grobéty B. 3D pore structure and ion conductivity of porous ceramic diaphragms. AIChE J. 2007;59(5):1446–1457.

[8] Gaiselmann G, Neumann M, Pecho O, Hocker T, Schmidt V, Holzer L. Quantitative relationships between microstructure and effective transport properties based on virtual materials testing. AIChE J. 2014;60(6):1983–1999.

[9] Petersen EE. Diffusion in a pore of varying cross section. AIChE J. 1958;4(3):343–345.

[10] Münch B, Holzer L. Contradicting geometrical concepts in pore size analysis with electron microscopy and mercury intrusion. J Am Ceram Soc. 2008;91(12):4053–4067.

[11] Diamond S. Mercury porosimetry: An inappropriate method for the measurement of pore size distributions in cement-based materials. Cem Concr Res. 2000;30(10):1517–1525.

[12] GeoDict - open source software. *www.geodict.com*. 2014.

[13] Hastie T, Tibshirani T, Friedman JH. The Elements of Statistical Learning. New York: Springer, 2008.

[14] Soille P. Digital Image Processing. Heidelberg: Springer, 2003.

[15] Avizo 7 - 3D analysis software for scientific and industrial data. *http://www.vsg3d.com/avizo/overview*. 2012.

[16] Thulasiraman K, Swamy MNS. Graphs: Theory and Algorithms. New York: John Wiley & Sons, 1992.

[17] Laarhoven PJM, Aarts EHL. Simulated Annealing: Theory and Applications. Dortrecht: Kluwer Academic Publisher, 1987.

[18] Pecho OM, Stenzel O, Iwanschitz B, Gasser P, Neumann M, Schmidt V, Prestat M, Hocker T, Flatt FJ, Holzer L. 3D microstructure of Ni-YSZ anodes: Prediction of effective transport properties and optimization of redox-stability. Materials 2015;8:5554–5585.

[19] Holzer L, Stenzel O, Pecho OM, Ott T, Boiger G, Gorbar M, De Hazan Y, Penner D, Schneider I, Cervera R and Gasser P. Fundamental relationships between 3D pore topology, electrolyte conduction and flow properties: Towards knowledge-based design of ceramic diaphragms for sensor applications; submitted to Mater Design.

[20] Becker J, Flückiger R, Reum M, Büchi F, Marone F and Stampanoni M. Determination of material properties of gas diffusion layers: experiments and simulations using phase contrast tomographic microscopy, J Electrochem Soc 2009; 156(10):B1175–B1181.

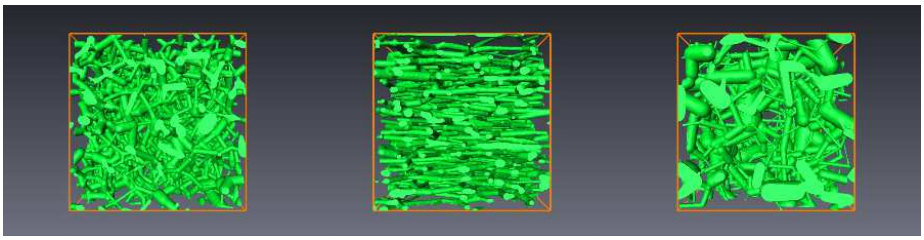

Figure 1: Virtual geometries generated by the stochastic microstructure model.

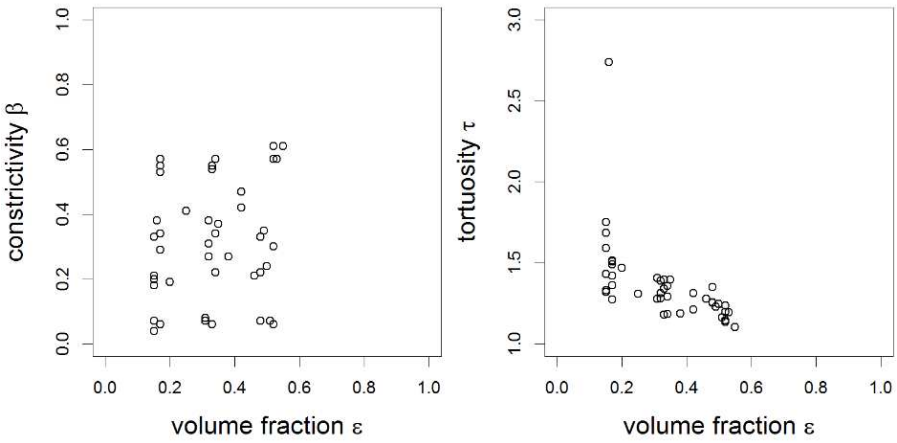

Figure 2: Geometric characteristics of the 43 microstructures.

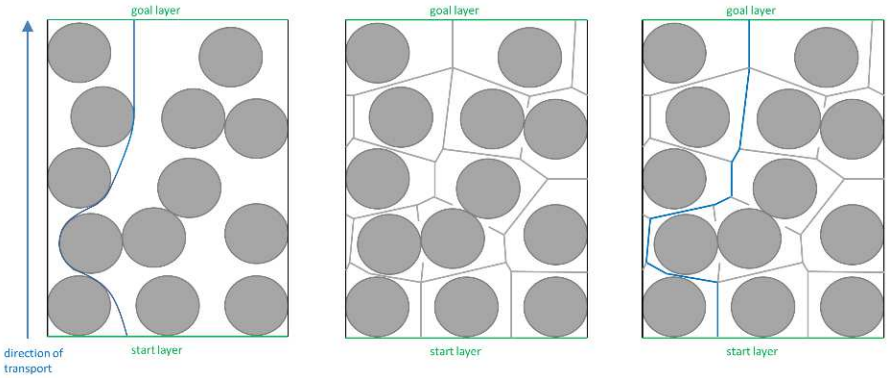

Figure 3: Illustration of two different tortuosity concepts. Left: The geodesic tortuosity τ_{geod} considers shortest pathways in the entire voxel-space representing the transporting phase (white). Center: Skeletonization of the transporting phase is the basis for geometric tortuosity. Right: Geometric tortuosity describes the lengths of shortest pathways on the skeleton network.

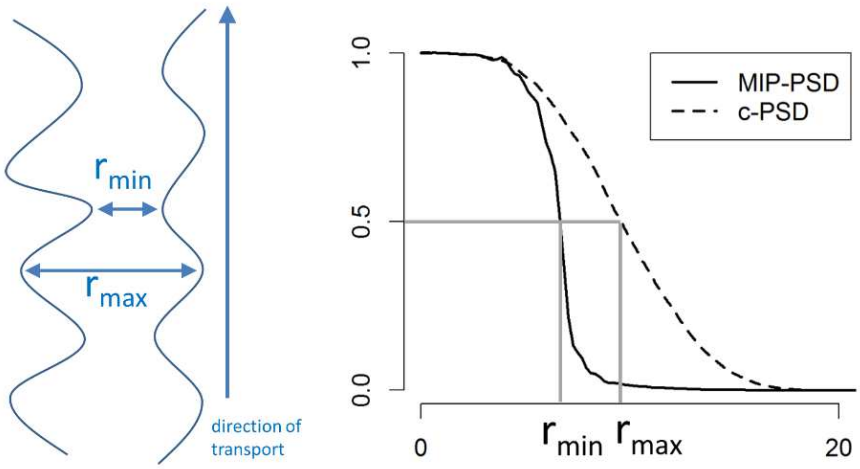

Figure 4: Left: basic idea of constrictivity $\beta = \left(\frac{r_{\min}}{r_{\max}}\right)^2$ with $r_{\min}$ as radius of typical 'bottleneck' and $r_{\max}$ as radius of typical 'bulge'. Right: example of c-PSD and MIP-PSD.

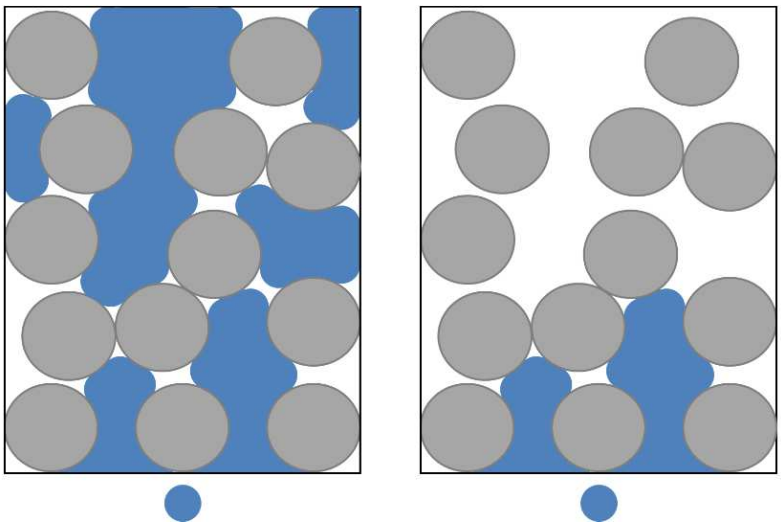

Figure 5: Illustration of c-PSD (left) and MIP-PSD (right). With the c-PSD concept a larger region can be filled with a sphere of given radius x. For MIP-PSD the intrusion at a capillary radius x from bottom to top is hindered by narrow bottlenecks with $r < x$.

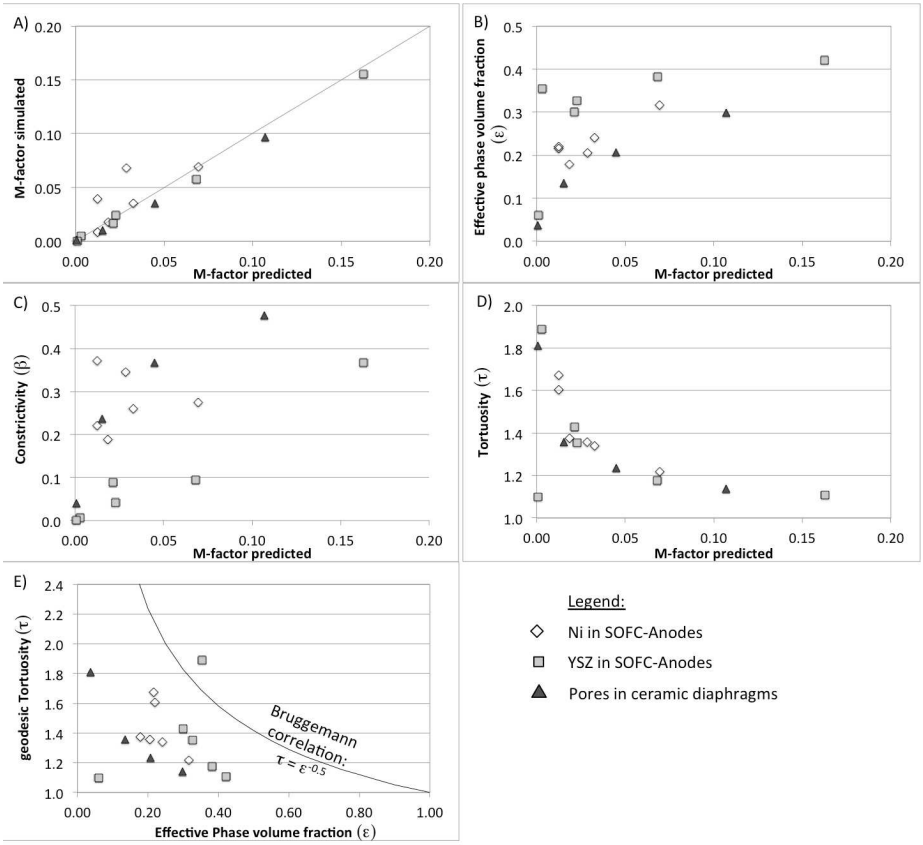

Figure 6: Validation based on tomography data of real samples from literature:[18,19] A) Validation of prediction using eq. (12). B)-D) Illustration of microstructure characteristics (phase volume fraction ε, tortuosity τ and constrictivity β. E) Relationship between geodesic tortuosity τ and volume fraction ε for experimental data.

List of Figures

Table 1: Results of statistical error minimization for 12 different prediction-equations. The parameters a, b, c, d are fitted for both, geodesic (left) and geometric tortuosities (right).

no.	eq.	geodesic tortuosity			geometric tortuosity		
		fitted	training error	prediction error	fitted	training error	prediction error
7	ε^b	$\varepsilon^{2.87}$	36.98 %	37.96 %	$\varepsilon^{2.87}$	36.98 %	37.96 %
8	$\frac{\varepsilon}{\tau^2}$	–	–	338.78 %	–	–	179.96 %
9	$\frac{\varepsilon\beta}{\tau^2}$	–	–	41.27 %	–	–	39.91 %
10	$\varepsilon^b\beta^c$	$\varepsilon^{2.28}\beta^{0.39}$	30.88 %	36.54 %	$\varepsilon^{2.28}\beta^{0.39}$	30.88 %	36.54 %
11	$\frac{\varepsilon^b}{\tau^d}$	$\frac{\varepsilon^{1.30}}{\tau^{5.52}}$	22.51 %	25.43 %	$\frac{\varepsilon^{2.23}}{\tau^{1.09}}$	33.31 %	41.32 %
12	$\frac{\varepsilon^b\beta^c}{\tau^d}$	$\frac{\varepsilon^{1.15}\beta^{0.37}}{\tau^{4.39}}$	16.16 %	19.06 %	$\frac{\varepsilon^{1.56}\beta^{0.45}}{\tau^{1.33}}$	22.61 %	26.39 %
13	$a\varepsilon^b$	$0.87\varepsilon^{2.72}$	36.93 %	41.96 %	$0.87\varepsilon^{2.72}$	36.93 %	41.96 %
14	$a\varepsilon^b\beta^c$	$1.07\varepsilon^{2.38}\beta^{0.39}$	30.81 %	38.69 %	$1.07\varepsilon^{2.38}\beta^{0.39}$	30.81 %	38.69 %
15	$\frac{a\varepsilon^b}{\tau^d}$	$\frac{0.87\varepsilon^{1.12}}{\tau^{5.68}}$	22.21 %	25.76 %	$\frac{1.82\varepsilon^{2.31}}{\tau^{2.01}}$	31.58 %	39.90 %
16	$\frac{a\varepsilon^b\beta^c}{\tau^d}$	$\frac{0.88\varepsilon^{1.06}\beta^{0.36}}{\tau^{4.35}}$	15.76 %	19.01 %	$\frac{2.08\varepsilon^{1.62}\beta^{0.49}}{\tau^{2.26}}$	15.24 %	17.24 %
17	$\frac{\varepsilon\beta^c}{\tau^d}$	$\frac{\varepsilon\beta^{0.36}}{\tau^{5.17}}$	16.36 %	17.69%	$\frac{\varepsilon\beta^{0.68}}{\tau^{2.21}}$	29.59 %	33.20 %
18	$\frac{\varepsilon^b\beta^c}{\tau^2}$	$\frac{\varepsilon^{1.67}\beta^{0.42}}{\tau^2}$	19.58 %	22.34 %	$\frac{\varepsilon^{1.29}\beta^{0.45}}{\tau^2}$	24.88 %	27.81 %

Table 2: Summary of prediction errors for various equations, whereby the bottleneck effect (i.e. constrictivity) was defined in three different ways (classes): using quantile ratios of only c-PSD, only MIP-PSD or both. For each of the three classes, the quantile ratio with the lowest prediction error is stated. In addition the errors when using conventional definition of constrictivity ($(r_{\mathrm{min}50}/r_{\mathrm{max}50})^2$) are also shown for comparison.

no.	eq.	error $\beta = \left(\frac{r_{\mathrm{min}50}}{r_{\mathrm{max}50}}\right)^2$	lowest error c-PSD	lowest error MIP-PSD	lowest error c-PSD & MIP-PSD
9	$\frac{\varepsilon\beta}{\tau^2}$	40.59%	40.88% $\leftrightarrow$ $\beta = \left(\frac{r_{\mathrm{max}75}}{r_{\mathrm{max}10}}\right)^2$	61.17% $\leftrightarrow$ $\beta = \left(\frac{r_{\mathrm{min}90}}{r_{\mathrm{min}10}}\right)^2$	39.40% $\leftrightarrow$ $\beta = \left(\frac{r_{\mathrm{min}25}}{r_{\mathrm{max}25}}\right)^2$
12	$\frac{\varepsilon^b\beta^c}{\tau^d}$	22.38%	29.17% $\leftrightarrow$ $\beta = \left(\frac{r_{\mathrm{max}90}}{r_{\mathrm{max}50}}\right)^2$	27.28% $\leftrightarrow$ $\beta = \left(\frac{r_{\mathrm{min}75}}{r_{\mathrm{min}50}}\right)^2$	21.17% $\leftrightarrow$ $\beta = \left(\frac{r_{\mathrm{min}90}}{r_{\mathrm{max}90}}\right)^2$
16	$\frac{a\varepsilon^b\beta^c}{\tau^d}$	18.54%	23.00% $\leftrightarrow$ $\beta = \left(\frac{r_{\mathrm{max}90}}{r_{\mathrm{max}10}}\right)^2$	24.12% $\leftrightarrow$ $\beta = \left(\frac{r_{\mathrm{min}90}}{r_{\mathrm{min}50}}\right)^2$	16.84% $\leftrightarrow$ $\beta = \left(\frac{r_{\mathrm{min}25}}{r_{\mathrm{max}25}}\right)^2$
17	$\frac{\varepsilon\beta^c}{\tau^d}$	25.55%	31.28% $\leftrightarrow$ $\beta = \left(\frac{r_{\mathrm{max}75}}{r_{\mathrm{max}25}}\right)^2$	28.13% $\leftrightarrow$ $\beta = \left(\frac{r_{\mathrm{min}75}}{r_{\mathrm{min}50}}\right)^2$	22.81% $\leftrightarrow$ $\beta = \left(\frac{r_{\mathrm{min}25}}{r_{\mathrm{max}25}}\right)^2$
18	$\frac{\varepsilon^b\beta^c}{\tau^2}$	25.38%	31.95% $\leftrightarrow$ $\beta = \left(\frac{r_{\mathrm{max}90}}{r_{\mathrm{max}50}}\right)^2$	29.13% $\leftrightarrow$ $\beta = \left(\frac{r_{\mathrm{min}75}}{r_{\mathrm{min}50}}\right)^2$	23.17% $\leftrightarrow$ $\beta = \left(\frac{r_{\mathrm{min}25}}{r_{\mathrm{max}25}}\right)^2$
averaged		26.49%	31.89% $\leftrightarrow$ $\beta = \left(\frac{r_{\mathrm{max}75}}{r_{\mathrm{max}10}}\right)^2$	37.24% $\leftrightarrow$ $\beta = \left(\frac{r_{\mathrm{min}90}}{r_{\mathrm{min}10}}\right)^2$	24.85% $\leftrightarrow$ $\beta = \left(\frac{r_{\mathrm{min}25}}{r_{\mathrm{max}25}}\right)^2$